

# SHAPE CONSTRAINTS IN SYMBOLIC REGRESSION USING PENALIZED LEAST SQUARES

VIKTOR MARTINEK<sup>✉</sup>, JULIA REUTER<sup>✉</sup>, OPHELIA FROTSCHER<sup>✉</sup>,  
SANAZ MOSTAGHIM<sup>✉</sup>, MARKUS RICHTER<sup>✉</sup>, AND ROLAND HERZOG<sup>✉</sup>

**ABSTRACT.** We study the addition of shape constraints and their consideration during the parameter estimation step of symbolic regression (SR). Shape constraints serve as a means to introduce prior knowledge about the shape of the otherwise unknown model function into SR. Unlike previous works that have explored shape constraints in SR, we propose minimizing shape constraint violations during parameter estimation using gradient-based numerical optimization.

We test three algorithm variants to evaluate their performance in identifying three symbolic expressions from a synthetically generated data set. This paper examines two benchmark scenarios: one with varying noise levels and another with reduced amounts of training data. The results indicate that incorporating shape constraints into the expression search is particularly beneficial when data is scarce. Compared to using shape constraints only in the selection process, our approach of minimizing violations during parameter estimation shows a statistically significant benefit in some of our test cases, without being significantly worse in any instance.

## 1. INTRODUCTION

Symbolic regression (SR) is a powerful, supervised machine learning approach to discover underlying mathematical expressions from data. The search space of potential expressions is very large, and the problem is NP-hard, as proven by [22]. However, there are ways to incorporate prior knowledge beyond the data into the expression search to guide the search more efficiently. One way to do this is by using shape constraints.

Shape constraints impose restrictions on the behavior (or shape) of a function. A relatively common example of a shape constraint is monotonicity with respect to some variable. Shape constraints can be used to incorporate domain-specific knowledge or enforce desired behavior, which can be very advantageous in many scenarios. For example, shape constraints can help reduce the required number of data, or help bridge regions where no data is available. In addition, shape constraints can mitigate the effect of noisy data, including data with outliers. Depending on how the shape constraints are implemented into the expression search, they can either provide additional guidance or even reduce the search space. These benefits have already been shown in several studies, including [11, 7, 8, 6, 3, 12,

---

*Date:* June 3, 2024.

*Key words and phrases.* symbolic regression, shape constraints, constrained least squares, thermodynamics, equations of state.

This work was funded by the Deutsche Forschungsgemeinschaft (DFG, German Research Foundation) – HE 6077/14-1 and RI 2482/10-1 – within the Priority Programme “SPP 2331: Machine Learning in Chemical Engineering”.

18, 19, 14]. Altogether, the expressions obtained have greater utility and reliability when they obey the domain-specific shape constraints.

Our proposed approach differs from previous work in two points. First, we take into account the amount of constraint violation already during the parameter identification step. To the best of our knowledge, this is only done in one other publication. Second, this parameter identification step is carried out using second-order optimization and algorithmic differentiation. This allows us to find a set of parameters such that the resulting model conforms to the constraints, while also fitting the data. As in other works, the constraint violations are implemented as additional objectives which are considered in the multi-objective selection process of the genetic algorithm.

In the following section, we briefly introduce the problem formulation of SR and extend it to include shape constraints. We describe our approach to the estimation of model parameters, which also minimizes the shape constraint violations. We then explain how we incorporate the shape constraints into the overall evolutionary algorithm. In Section 3, related works are briefly described and the differences to the present work are outlined in more detail. In Section 4, the experiments are detailed, and their results presented. Section 5 offers a summary and discussion of the results. Finally, we draw a conclusion in Section 6.

## 2. SHAPE CONSTRAINTS IN SR

In SR, the goal is to find a mathematical expression  $m$ , along with values for its parameters  $p$ , such that we

$$(2.1) \quad \text{Minimize} \quad \frac{1}{N} \sum_{i=1}^N f\left(\frac{y_i - m(X_i, p)}{y_i}\right) \quad \text{w.r.t. } (m, p).$$

The expression  $m$  comes from an admissible class of expressions ensuring its syntactic correctness. The parameter  $p$  is from a parameter space that generally depends on  $m$ . Above, the vector-valued  $X$  and the scalar-valued  $y$  are the independent and dependent variables of the model, and  $(X_i, y_i)$  denote the pairs of data in the data set,  $i = 1, \dots, N$ . The function  $f$  is known as loss function and typical examples include  $f(r) = r^2$ , leading to (2.1) representing the mean squared relative error.

Currently, genetic programming algorithms perform best among wide-ranging SR tasks (see [13]). Summarized briefly, the population-based genetic programming algorithms combine candidate expressions (crossover), and insert slight variations into candidate expressions (mutation). In this way, new candidate expressions are generated. Better candidate models replace less favorable ones in the population, which is known as the selection process.

As shorter and intuitively simpler expressions are preferred, problem (2.1) is augmented by an additional objective measuring the complexity, e.g., length, of the expression  $m$  in most SR approaches. Many approaches consider additional objectives, such as age (see [21]), or the coefficient of determination  $R^2$ .

In any case, (2.1) becomes a multi-objective problem. Depending on the algorithm, these competing objectives are either addressed through the concepts of Pareto dominance, or aggregated to a yield singular fitness value by means of a weighted sum.

In this work, we use thermodynamics-informed symbolic regression (TiSR) (see [15]), an SR implementation based on NSGA-II (see [5]). In contrast to NSGA-II, TiSR uses both Pareto dominance and fitness-based selection criteria to ensure sufficient diversity in the population. TiSR is written in JULIA (see [1]) and available at <https://github.com/scoop-group/TiSR>.

Shape constraints are expressed by augmenting problem (2.1) using inequality and/or equality constraints. The problem then becomes

$$(2.2) \quad \begin{aligned} & \text{Minimize} && \frac{1}{N} \sum_{i=1}^N f\left(\frac{y_i - m(X_i, p)}{y_i}\right) && \text{w.r.t. } (m, p) \\ & \text{subject to} && g(m(X, p)) \leq 0 && \text{for all } X \in \Omega, \\ & && \text{and } h(m(X, p)) = 0 && \text{for all } X \in \Omega. \end{aligned}$$

The set  $\Omega$  defines the range for the independent variable  $X$  on which the constraint is relevant. Therefore, in general, there are infinitely many constraints, that can be taken into account in two different ways.

In pessimistic approaches, interval arithmetic is used to compute an enclosure of the range of the constraint function's values over  $X \in \Omega$ . This offers algorithms the possibility to certify a model's feasibility w.r.t. all constraints. However, such approaches may deem feasible models infeasible, as observed and discussed by Haider et al. (see [8]).

By contrast, optimistic approaches evaluate and enforce the constraints only in a finite number of predetermined locations. While this may lead to models incorrectly classified as feasible, the evaluation of constraints as well as their derivatives w.r.t.  $p$  is straightforward.

In this study, we employ an optimistic approach. The constraint evaluation points  $X^1, \dots, X^C$  are distinct from the data points  $X_1, \dots, X_N$ . In order to accommodate different types of constraints, the constraint functions  $g$  and  $h$  can be vector-valued. This allows several shape constraints to be considered simultaneously, e. g., monotonicity and bounds on the function values.

The parameters  $p$  of each candidate model can be identified using the same evolutionary mechanisms that are used to drive model evolution, as exemplified by Koza in the early literature on genetic programming for SR (see [10]). However, most contemporary SR algorithms treat the parameter identification as a subordinate problem, employing gradient-based fitting for each candidate model before the loss in (2.1) is determined. Kommenda et al. have shown the benefits associated with this approach (see [9]).

Using  $f(r) = r^2$ , the parameter identification subproblem, i. e., (2.2) with the model  $m$  fixed, becomes a constrained least-squares problem. Despite the relevance of this problem class in many industrial and academic fields, we were unable to find an appropriate open-source implementation of a constrained least-squares problem solver.

We therefore employ a penalty approach. Given a model with parameters  $p$ , we measure the total violation of the constraints in terms of the  $\ell_2$ -squared penalty, i. e.,

$$(2.3) \quad \sum_k \sum_{\ell=1}^C h_k(m(X^\ell, p))^2 \quad \text{and} \quad \sum_k \sum_{\ell=1}^C \max(0, g_k(m(X^\ell, p)))^2.$$

These values represent the extent to which the constraints are violated at the points of evaluation. Notice that the constraint evaluation points  $X^1, \dots, X^C$  are the same for each constraint in (2.3). This is merely for the sake of notational convenience. In our implementation, we allow the constraint evaluation points to be different for each component  $h_k$  and  $g_k$  of the constraint functions.

During the parameter identification step in our algorithm, we minimize a weighted sum of the loss and the constraint violation (2.3). In order to keep the computational expense limited, we work with a fixed penalty parameter. We use the NEWTON implementation of the JULIA library OPTIM.JL (see [17]) for this purpose. First- and second-order derivatives of the loss as well as the constraints are provided through the algorithmic differentiation package FORWARDDIFF.JL (see [20]). This is an essential distinction from [12], where Monte-Carlo-based multiobjective local search is used for parameter fitting. Gradient-based approaches, where available, often outperform non-deterministic approaches (see [16]).

With the parameter values optimized, there are at least two distinct ways for an evolutionary algorithm to take into account the amount of constraint violation encountered in a particular model. In so-called hard-constrained approaches, candidate models are removed from the population in case they are infeasible. By contrast, soft-constrained approaches incorporate constraint violations through one or several additional objectives. Hard constraints may lead to a loss of diversity in the population, which is essential for evolutionary algorithms, while soft constraints allow to improve upon the candidate in later generations.

Haider et al. compared hard- and soft-constrained approaches and found no statistically significant differences between them (see [7]). We therefore choose to implement a soft-constrained approach, where the two terms in (2.3) are added to form a single additional objective.

### 3. RELATED WORK

In an early work, [14] introduced asymptotic constraints into SR, controlling the function behavior at zero and infinity. They utilized a neural network to guide their Monte-Carlo tree search-based method and to produce expressions with the desired asymptotic behavior. Although effective through restriction of the search space, it is not directly applicable to other types of constraints.

[2, 3] use a satisfiability modulo theories (SMT). The SMT solver guarantees that solutions are feasible, resembling a pessimistic approach. The types of constraints considered include bounds on function values and partial derivatives, as well as symmetries and periodicity. Their approach, namely ‘‘Counterexample-Driven Genetic Programming’’, also maintains a training set with counter examples, which is continuously extended during the expression search. On the downside, SMT solvers may be computationally prohibitive and do not support all types of constraints.

Closest to our approach in the present work is [12]. The constraints are evaluated on a finite number of sample points. Notably and similar to our approach, the shape constraints are part of the parameter identification subproblem. Contrary, however, they use a multi-objective local search procedure based on Monte-Carlo methods for this problem.

[11] introduce a new approach to shape-constrained SR. They use interval arithmetic to check constraint satisfaction in a pessimistic manner. Their study is limited to box constraints on the function values and its partial derivatives. Two approaches

of incorporating the shape constraints into the expression search are studied. One uses hard constraints, while the other maintains separate populations for feasible and infeasible candidates. In contrast to our work, the constraint violations are not part of the parameter identification subproblem.

[7] employs soft constraints which allows the constraint violation to be reduced over multiple generations. The authors utilize three different evolutionary algorithms as a basis and study various ways of treating and incorporating shape constraints into the expression search. The benefits of shape constraints, e. g., for noisy data, are clearly shown. Interestingly, the authors conclude that in all their experiments, there are no statistically significant differences between the core algorithms nor among the approaches to incorporate the shape constraints.

[8] compare optimistic and pessimistic constraint evaluation approaches. The authors conclude that optimistic approaches may improve the extrapolation behavior of models, while pessimistic approaches seem to be better suited for higher levels of noise.

#### 4. EXPERIMENTS

We conduct experiments on three different benchmark problems. In each case, a ground truth model is known and used to generate synthetic data. The goal of our experiments is to study the utility in using shape constraints to reconstruct the ground truth model. In contrast to previous works, we do not emphasize the effects of shape constraints on the composition of the final Pareto frontier (hall of fame).

In what follows, we first detail how we set up our proposed method and two baseline methods we compare our method to. This is followed by a description of the three benchmark problems. For each, the ground truth expressions and the sample ranges over which the synthetic data used for fitting are shown. Also, the constraints used for each problem as well as sample ranges for the constraints evaluation points are specified.

**4.1. Description of Algorithmic Variants.** We describe three algorithmic variants. All variants are implemented in TiSR. (1) As a first baseline (**base**), we use TiSR without shape constraints. (2) The second baseline (**obj**) takes shape constraints into account partially. As in **base**, it solves the parameter identification problem for each model without considering the shape constraints. It then evaluates the constraint violation (2.3) and introduces the combined amount of violation as a separate, additional objective. This approach resembles the one of Haider et al. (see [7]). (3) The third variant (**minim\_obj**) alters the parameter identification step. It first identifies them without considering the constraints, like both baseline methods. If certain criteria are met (mentioned below), the parameter identification is continued using the penalty-based constrained least squares. The constraint violations after the parameter identification are used for the selection, like in **obj**.

Most of TiSR’s default parameters are used in all three variants. To minimize the mean squared relative error, as shown in (2.1), the `fit_weights` parameter is set to  $1/t_i$  for each residual value  $r_i$ , where  $t_i$  is the value of the target, or dependent variable for datum  $i$ . The maximum complexity, i. e., the number of operators and operands allowed for candidate expressions, is set to 5 above the reference ground truth expression.

The default selection objectives of TiSR [`:ms_processed_e`, `:compl`, `:age`] are the mean squared error, complexity of the expression (number of operators and

operands), and age of the expression (number of generations it has been present in the population). For the purpose of the present study, we extend these objectives by `:minus_abs_spear` and `:constr_vios`. Here `:minus_abs_spear` is the negative of the absolute of the Spearman correlation, which is added as a supporting objective as defined in [23]. The `:constr_vios` objective contains the sum of the constraint violations as in (2.3), which is always zero for the `base` variant of the algorithm. The default hall of fame objectives [`:ms_processed_e`, `:compl`, `:mare`] are extended by `:constr_vios`. The `:mare` objective represents the mean absolute relative error, which is calculated as in (2.1), but with loss function  $f(r) = |r|$  in place of  $f(r) = r^2$ . Further parameters of TiSR that deviate from their defaults are summarized in Table 4.1.

TABLE 4.1. Overview and description of some of TiSR’s parameters set for all experiments, deviating from their default values.

Parameter	Value	Description
<code>t_lim</code>	60*10	TiSR is allowed to run for a maximum of ten minutes.
<code>pop_size</code>	500	The population size, i. e., the number of candidate models in the population, is set to 500.
<code>pow_abs_param</code>	<code>true</code>	The power operator ( $\wedge$ ) can only have parameters in its exponent. Variables or expressions are not allowed as exponents.
<code>always_drastic_simplify</code>	1e-7	Candidate models containing parameters that are closer to one or zero than $10^{-7}$ are simplified by rounding the respective parameters to one or zero.
<code>max_iter</code>	30	The parameter identification is allowed to take up to 30 iterations.

All three algorithmic variants are allowed to use up to 30 iterations for each parameter identification subproblem. In fact, the `base` and `obj` variants use a Levenberg-Marquardt method for this purpose. The third variant `minim_obj` allots a budget of up to 20 Levenberg-Marquardt iterations without constraint penalization. Provided that the mean absolute relative error is smaller than the pre-selected parameter `max_mare_for_constr_fit`, an additional maximum of 10 Newton iterations of the problem with constraint penalization follow. The parameter `max_mare_for_constr_fit` is set 5% higher than set the noise level of the data. The constraint penalty coefficient `constr_penalty_factor` is fixed and set to 1.

**4.2. Verification of Results.** To efficiently check whether the ground truth is reconstructed, a separate verification data set is used. This verification data set is sampled separately using the ground truth expression, on a wider range than the original data set, and using 2 to 5 times as much data. Approximately every 5 s, all candidate solutions in the hall of fame are passed to a callback function. Those with a mean absolute relative error of at most 5% higher than the noise level of the data are fitted to the verification data set. If the mean absolute relative error with

respect to the verification data set is lower than 0.0001 %, the expression search is terminated with success. We recall that only expressions with a complexity of up to 5 above the reference ground truth expression can be accepted. The expression search does not gain any information from the verification data set or the callback overall.

**4.3. Description of the Benchmark Problems.** We report on three different problems, each using a different ground truth expression. In all cases, no part of the expression nor its parameters are initially known to TiSR. Every problem has two independent and one dependent variable.

**4.3.1. Gaussian Distribution.** The first problem (`gaussian`) is the density of a univariate Gaussian distribution with the mean fixed at 0:

$$(4.1) \quad y = \frac{\exp\left(-\frac{\theta^2}{2\sigma^2}\right)}{\sqrt{2\pi}\sigma}.$$

The independent variables  $\sigma$  and  $\theta$  denote the standard deviation and the probability density, respectively. A graph illustrating Equation (4.1) is shown in Figure 4.1. The ground truth expression has a complexity of 11 operators and operands.

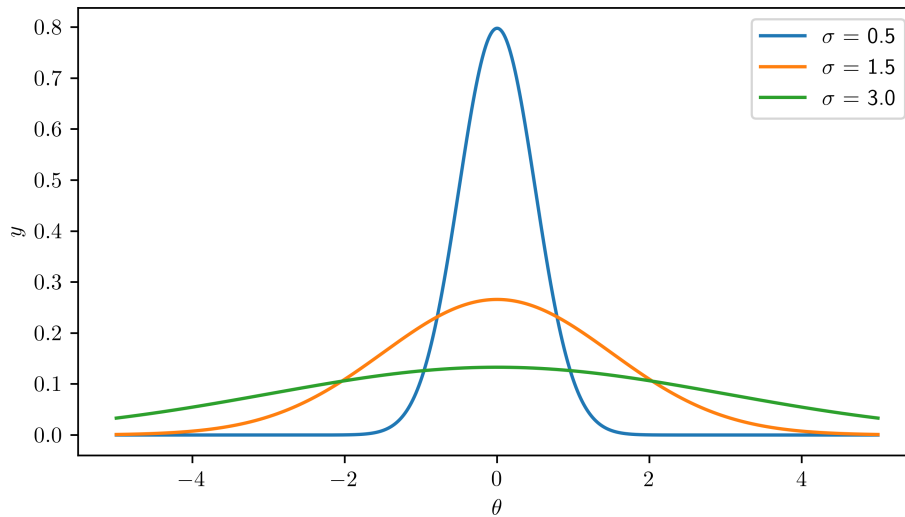


FIGURE 4.1. Plot of the Gaussian normal distribution for varying standard deviation  $\sigma$  and random variable values  $\theta$ .

For all variables, ranges are defined and within those, 100 points uniformly, randomly sampled. The ranges for the fitting data set are  $[-5, 5]$  for  $\theta$ , and  $[0.5, 3]$  for  $\sigma$ . For the verification data set, 500 points are sampled within the ranges of  $[-10, 10]$  and  $[0.5, 5]$  for  $\theta$  and  $\sigma$ , respectively. The function set for this expression is set to  $[+, -, *, /, \wedge, \exp, \text{pow2}, \text{sqrt}]$ , where `pow2` is a unary function raising to the power of 2.

Although more are possible, we define constraints on the function values and the first derivatives of the function. The constraints on the function value are summarized in Table 4.2, while the constraints on the first derivatives are listed in

**Table 4.3.** For each of those, five points are sampled for each variable individually. Then 5  $(\theta, \sigma)$  pairs are randomly drawn from the total of the 25 potential pairs. These constraint evaluation points remain the same during each run but may differ between runs.

TABLE 4.2. Treatment of the function value constraints for the gaussian benchmark problem.

$\theta$ sample parameters	$\sigma$ sample parameters	constraint
logarithmically in $[-100, -0.01]$	uniformly in $[0.5, 6]$	$f \geq 0$
logarithmically in $[0.01, 100]$	uniformly in $[0.5, 6]$	$f \geq 0$

TABLE 4.3. Treatment of the monotonicity constraints for the gaussian benchmark problem.

$\theta$ sample parameters	$\sigma$ sample parameters	constraint
logarithmically in $[-0.01, -100]$	uniformly in $[0.5, 6]$	$\partial f / \partial \theta \geq 0$
logarithmically in $[0.01, 100]$	uniformly in $[0.5, 6]$	$\partial f / \partial \theta \leq 0$
$\{0\}$	uniformly in $[0.5, 6]$	$\partial f / \partial \sigma \leq 0$

4.3.2. *Magnetic Manipulator Force.* The second expression we use in our experiments is also used by [12] for their study of SR with shape constraints. It describes the force exerted by an electromagnet on an iron ball moving along a rail in a magnetic manipulator system (**magman**). The expression is

$$(4.2) \quad F = \alpha \cdot \frac{x \cdot I}{(x^2 + \beta)^3},$$

where the independent variables  $x$  and  $I$  denote the distance and the current, and the parameters  $\alpha$  and  $\beta$  are system specific parameters. For  $(\alpha, \beta)$ , we adopt values  $(5.25, 1.75)$  identified by [4]. The resulting function (4.2) is shown in Figure 4.2. The ground truth expression has a complexity of 11 operators and operands.

For the distance  $x$ , the variable range for the fitting data set is  $[-3, 3]$ , while we take  $[-6, 6]$  for the verification data set. The ranges for the current  $I$  are  $[0.1, 0.8]$  and  $[0.1, 1.6]$  for the fitting and the verification data set, respectively. The function set is composed of  $[+, -, *, /, \wedge, \text{pow2}, \text{pow3}]$ , where **pow3** is a unary function raising to the power of 3.

Similarly as in the case of the **gaussian** problem, function value and monotonicity constraints are defined for **magman**. The function value constraints are summarized in Table 4.4, while the constraints on the first derivatives are listed in Table 4.5. The selection of constraint evaluation points is the same as described for the **gaussian** problem.

4.3.3. *Van der Waals Force.* The third used expression is the Van der Waals thermodynamic equation of state (**vanderwaals**). It models the pressure  $p$  of a fluid as a function of the molar volume  $v$  and the temperature  $T$  as independent variables:

$$(4.3) \quad p = \frac{R \cdot T}{v - b} - \frac{a}{v^2}.$$



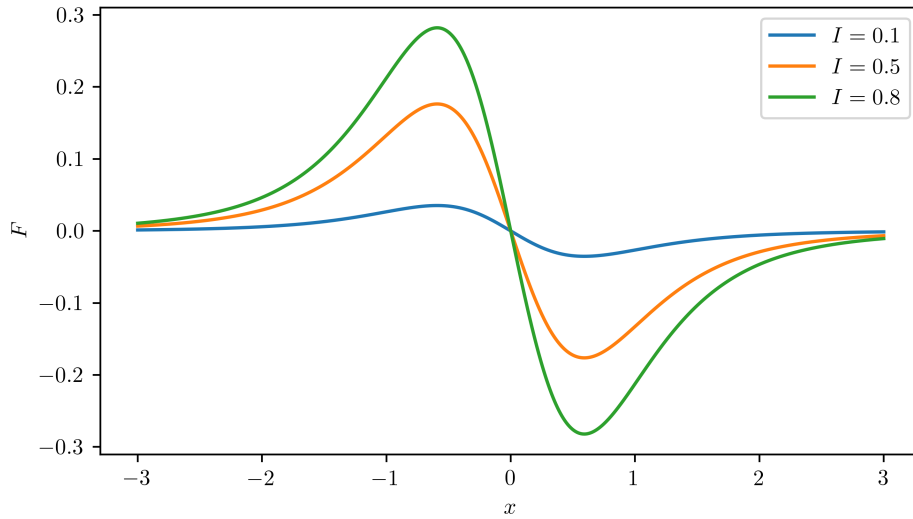


FIGURE 4.2. Plot of the force  $F$  exerted by a magnetic manipulator on an iron ball moving along rails for varying distances  $x$  and varying current  $I$ .

TABLE 4.4. Treatment of the function value constraints for the `magman` benchmark problem.

$x$ sample parameters	$I$ sample parameters	constraint
logarithmically in $[-1000, -0.1]$	uniformly in $[0.1, 0.8]$	$f \geq 0$
logarithmically in $[0.1, 1000]$	uniformly in $[0.1, 0.8]$	$f \leq 0$

TABLE 4.5. Treatment of the monotonicity constraints for the `magman` benchmark problem.  $r_1$  and  $r_2$  are the analytically determined roots of the first derivative of the `magman`, expression at approximately  $-0.592$  and  $0.592$ .

$x$ sample parameters	$I$ sample parameters	constraint
logarithmically in $[-10, r_1]$	uniformly in $[0.1, 0.8]$	$\partial f / \partial x \geq 0$
uniformly in $[r_1, r_2]$	uniformly in $[0.1, 0.8]$	$\partial f / \partial x \leq 0$
logarithmically in $[r_2, 10]$	uniformly in $[0.1, 0.8]$	$\partial f / \partial x \geq 0$
logarithmically in $[-50, -0.1]$	uniformly in $[0.1, 0.8]$	$\partial f / \partial I \geq 0$
logarithmically in $[0.1, 50]$	uniformly in $[0.1, 0.8]$	$\partial f / \partial I \leq 0$

Here  $R \approx 8.3145$  is the universal gas constant, and  $a$  and  $b$  are fluid-specific parameters. We use data for methanol, where the parameters  $(a, b)$  are  $(0.9649, 6.702 \cdot 10^{-5})$ . Figure 4.3 shows the function (4.3). The ground truth expression has a complexity of 12 operators and operands.

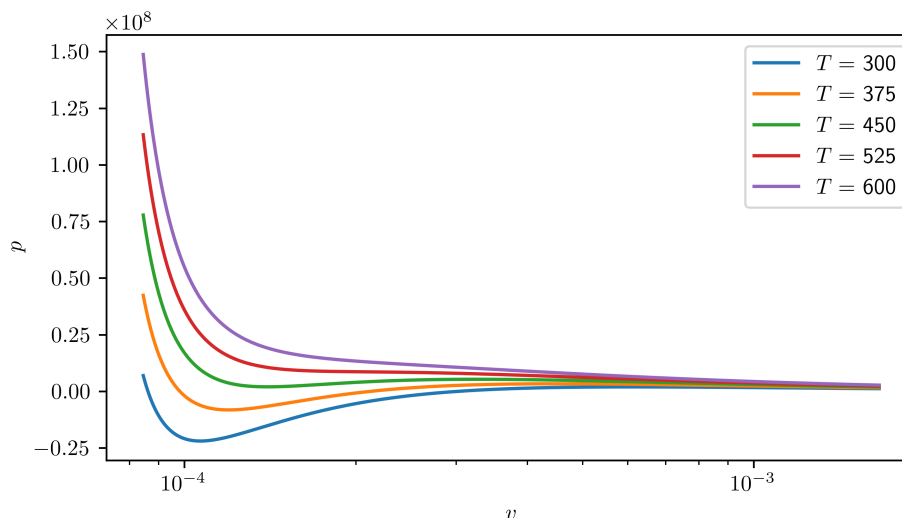


FIGURE 4.3. Plot of the Van der Waals thermodynamic equation of state. The pressure  $p$  is shown for varying temperatures  $T$  and specific volumes  $v$ .

We choose the `vanderwaals` problem since it involves a relatively complex shape constraint, allowing us demonstrate the capabilities and potential of our approach to incorporate shape constraints. The shape constraint for this problem originates from the Maxwell criterion, as it is commonly enforced in thermodynamic equations of state to enable the calculation of the vapor-liquid phase-boundary. For states  $(T, v)$  inside the two-phase region, the pressure calculated by such equations has to be disregarded. Instead, the pressure along isotherms is constant throughout the two-phase region. We briefly summarize the essence to understand the constraint without going into the thermodynamic detail. In Figure 4.4, the integral of the function along the isotherm (blue line) shifted by the entry points to the two-phase region (red line) must be zero in-between the entry points (red cross).

We generate three equidistant, regular grids for the `vanderwaals` expression, one in the vapor phase, one in the liquid phase, and one in the supercritical phase. To obtain a more realistic grid, the variable ranges are defined to  $T$  and  $p$  rather than  $T$  and  $v$ , as is common in experimental practice. The variable ranges are  $T = [450, 500]$ ,  $p = [0.05 \cdot 10^6, 2 \cdot 10^6]$  for the gas phase,  $T = [300, 400]$ ,  $p = [6 \cdot 10^6, 7 \cdot 10^6]$  for the liquid phase, and  $T = [550, 600]$ ,  $p = [10 \cdot 10^6, 11 \cdot 10^6]$  for the supercritical phase. Instead of random sampling, the data are sampled equidistantly on regular grids in each of the three ranges. Additionally, four phase transitions points are added to the fitting data set. These points are used in the Maxwell criterion constraint, and thus assumed to be known exactly. Their values and usage in the constraints are shown below. There are 147 points in the fitting data set, and 300 in the verification data set.

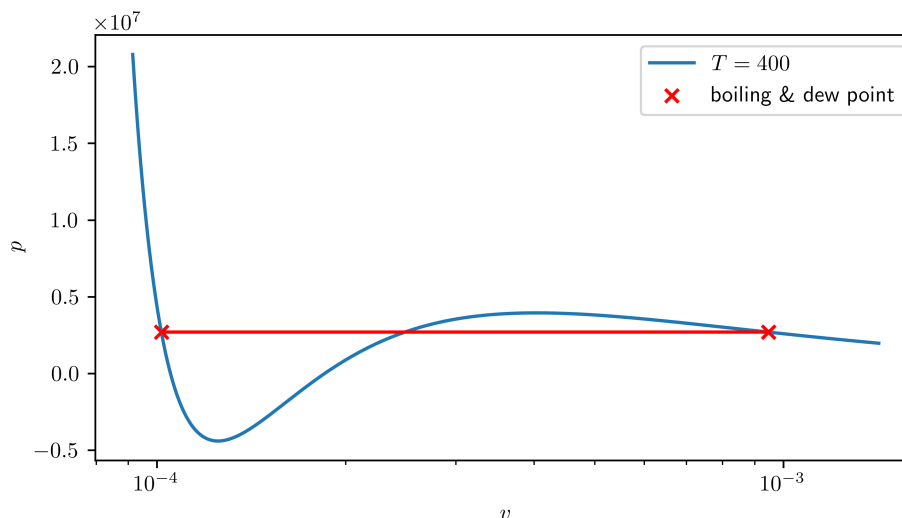


FIGURE 4.4. Pressure  $p$  plotted over molar volume  $v$  at a temperature of  $T = 400$  covering the two-phase region generated using the `vanderwaals` expression. The boiling and dew points are shown and connected with a red line. The Maxwell criterion requires the integral of the difference of the two function to be zero between the boiling and dew points.

The Maxwell criterion is incorporated as an equality constraint. The exact phase transition states are specified inside the constraint, marking the numerical integration bounds and the pressure-shifts for two isotherms. To reduce the computationally expensive numerical integration, the constraint has two parts. Before assessing the Maxwell criterion in the second part of the constraint, the deviations from the phase-transition states are assessed and also treated as equality constraints. Only for mean absolute relative error to the transition states below 1.00 %, the expensive numerical integration is conducted, the Maxwell criterion checked, and the violation added to the one described above. To ensure a descent in the transition from the first to the second part of the constraint, a dummy penalty of 1000 is added to the mean absolute relative error, while the results of the integration are divided by 1000. This fix does not render the transition smooth, but ensures a descent in this case, and is worth the computational expense saved. For the isotherms  $T_1 = 300$  and  $T_2 = 400$ , the pressure offsets are  $p_1 \approx 595\,000$  and  $p_2 \approx 2.70 \cdot 10^6$ . The specific volumes at the two-phase transitions, which mark the integration bounds, are  $v_{1,\text{boiling}} \approx 8.61 \cdot 10^{-5}$  and  $v_{1,\text{dew}} \approx 0.00385$  for  $T_1$ , and  $v_{2,\text{boiling}} \approx 0.000102$  and  $v_{2,\text{dew}} = 0.000947$  for  $T_2$ .

**4.4. Increasing Noise Levels.** We conduct two studies using the three algorithmic variants and the three benchmark problems. In the first, the resilience to noise is studied by applying varying noise levels on the dependent component of each data set. We use normally distributed random noise scaled by the respective target

to model relative noise. The noise levels, i. e.,  $\ell = \{0.1, 0.3\}$ , are applied using

$$(4.4) \quad t_i^{\text{noisy}} = t_i + t_i \cdot \mathcal{N}(0, 1) \cdot \ell,$$

for each datum  $i$ . Each algorithm-noise level combination is run for 31 times for statistical comparison. The results are shown in Figure 4.5.

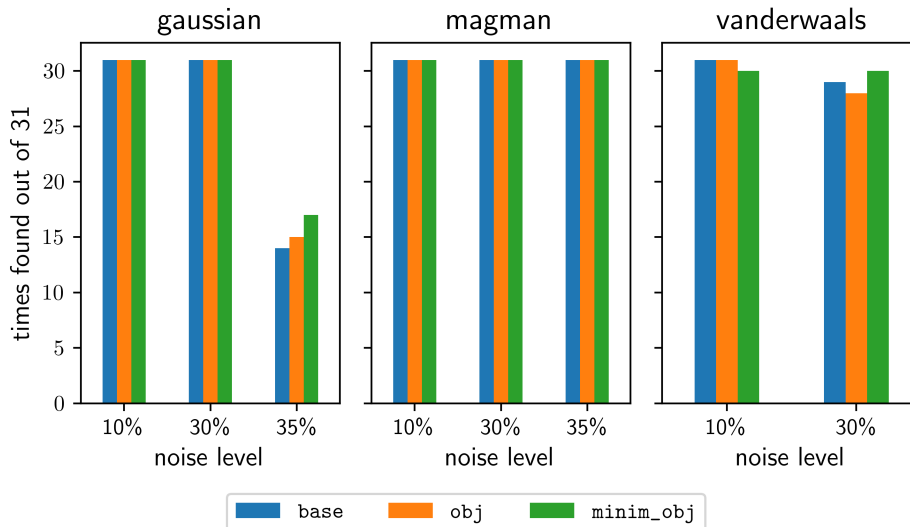


FIGURE 4.5. Times out of 31 that each of the three algorithmic variants (`base`, `obj`, `minim_obj`) find each of the three ground truth expressions (`gaussian`, `magman`, `vanderwaals`) for noise levels of 10%, 30%, and 35% noise levels.

For 10% and 30% noise, all variants are successful between 28 and 31 times out of 31 runs. Also, for the `magman` expression search at 35% noise level, all variants find the expression in all runs. At 35% noise for the `gaussian` expression, `base` finds the expression only 14 times, while `obj` and `minim_obj` find it 15 and 17 times, respectively. The two-proportion z-test with a confidence level of 5% is used to determine whether there are statistically significant differences for the three algorithms. For this study, the three algorithmic variants do not exhibit statistically significant differences.

**4.5. Reducing Data.** In the first part of the second study, we fix the noise level to  $\ell = 0.1$  but successively reduce the data available for fitting. We filter the data sets, by removing the data closest to the normalized center of the data, thus creating a “data hole”. First, data is normalized by dividing each datum  $x_{ij}$  by the maximum datum of its column  $j$ :

$$(4.5) \quad x_{ij}^{\text{norm}} = \frac{x_{ij}}{\max(x_j)}$$

Thereafter, the normalized center  $\mu_j$  for each column  $j$  is determined using

$$(4.6) \quad \mu_j = \frac{1}{n} \sum_{i=1}^n x_{ij}^{\text{norm}}.$$

The data with the highest Euclidean distance to the normalized center, calculated by

$$(4.7) \quad d_i^2 = \sum_{j=1}^m (x_{ij}^{\text{norm}} - \mu_j)^2,$$

is removed last. Each experiment is repeated ten times. The study is conducted for the **gaussian** and the **magman** expression. The results are shown in Figure 4.6 and Figure 4.7.

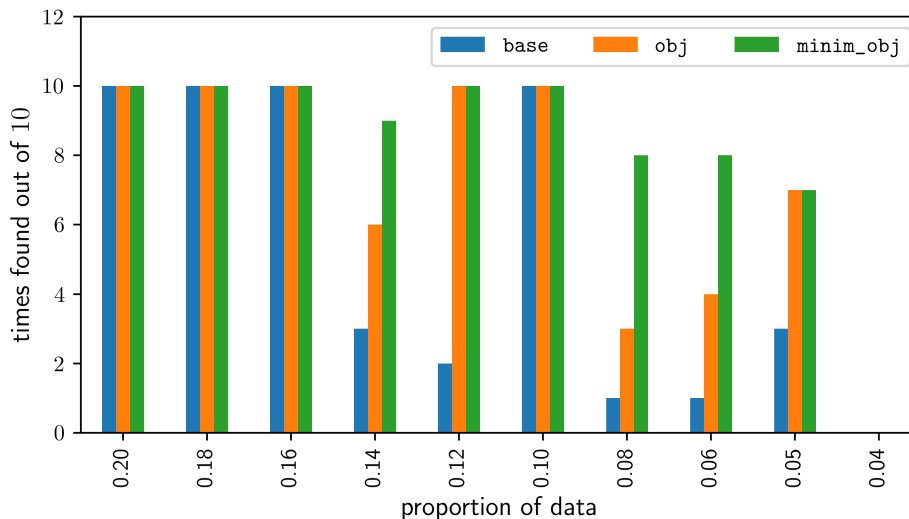


FIGURE 4.6. Times out of ten that each algorithmic variant finds the **gaussian** expression at 10% noise level for different proportions of data out of 100 data points.

First, the significant results for the **gaussian** benchmark problem (see Figure 4.6) are discussed. Assuming a significance level of 5.00%, for 14 points, **minim\_obj** is statistically significantly better than **base**, but not statistically significantly better than **obj**. Also, **obj** is not statistically significantly better than **base** in this case. At twelve points, both **obj** and **minim\_obj** are statistically significantly better than **base**. For eight points, **minim\_obj** is statistically significantly better than the other two variants, while **obj** is not significantly better than **base**. For six points, the only statistically significant result is that **minim\_obj** is better than **base**. At five and four points, none of the results are statistically significant.

Figure 4.7 shows the same experiments for the **magman** expression. For 40 and 35 points, **obj** and **minim\_obj** are significantly better than **base**, while not being statistically significantly different. At 30 points, **obj** is significantly better than **base**, while **minim\_obj** is not. However, **obj** is not statistically significantly better than **minim\_obj**.

For the **vanderwaals** expression, the data are reduced in a different manner. As mentioned above, the initial **vanderwaals** data set consists of three regular grids in three phases, i. e., the gas phase, the liquid phase, and the critical phase.

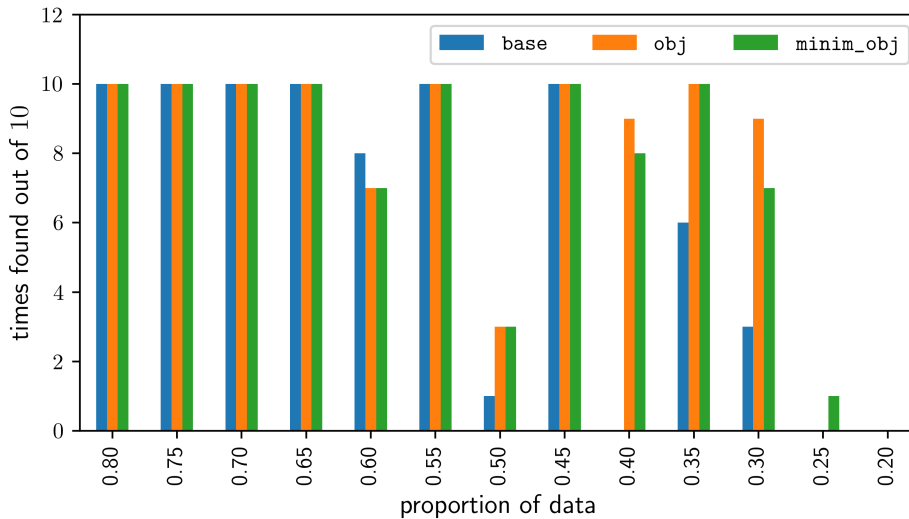


FIGURE 4.7. Times out of ten that each algorithmic variant finds the **magman** expression at 10% noise levels for different percentages of data out of 100 data points.

Additionally, four points at the vapor and dew line are included in the data set, where no noise is added, regardless of set the noise levels. For this part of the study, only the data in the liquid phase and the additional points are kept. Ten experiments are conducted with each, 0% and 10% noise levels. The results are shown in Figure 4.8.

None of the results show statistically significant differences.

## 5. SUMMARY AND DISCUSSION

In Section 4, we compare three algorithmic variants that differ in the way they incorporate used-defined shape constraints: (1) The first baseline variant (**base**) does not consider shape constraints at all. (2) The second baseline variant (**obj**) likewise uses unconstrained least squares for the parameter identification subproblem and subsequently uses the constraint violation for the purpose of selection. This resembles the algorithm proposed by Haider et al. (see [7]). (3) The third, proposed variant (**minim\_obj**) already incorporates the constraint violation into the parameter optimization step. Our implementation of all three variants are based on SR library TiSR.

Several experiments are conducted to test the resilience to noise and to a reduction of the amount of available data. The data is synthetically generated from ground truth expressions. The experimental setup, including the verification step, allows us to evaluate the differences between the three algorithmic variants with respect to their capability of recovering the ground truth models exactly.

With regard to the noise level, our experiments indicate that the algorithmic variants that utilize shape constraints (**obj** and **minim\_obj**), do not show significant benefits compared to **base**. With regard to the amount of data, however, the two variants **obj** and **minim\_obj** do exhibit statistically significant benefits compared

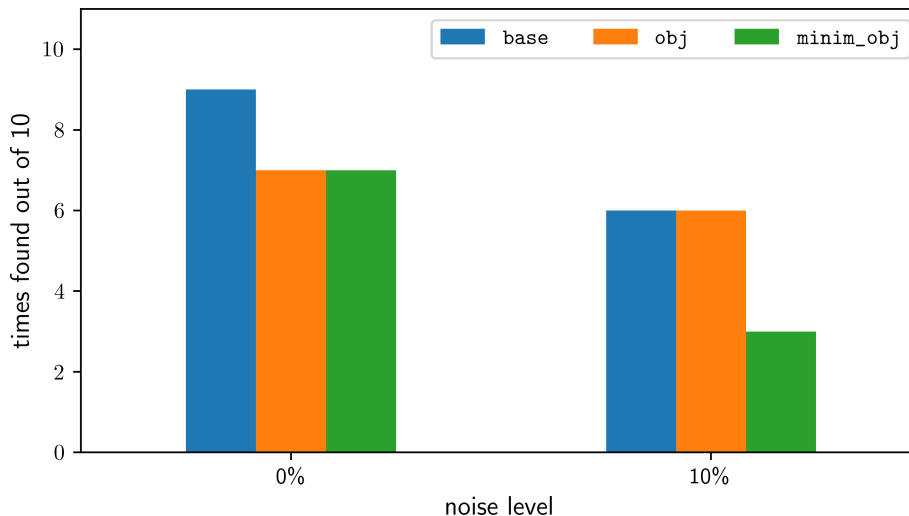


FIGURE 4.8. Times out of ten that each algorithmic variant finds the `vanderwaals` expression using only data from the liquid phase and four phase transition points at 0% and 10% noise levels.

to `base`. Among the two, our proposed approach `minim_obj` outperforms `obj` in a few cases with statistical significance.

Admittedly, we expected our proposed approach to stand out more clearly. This might be due to several reasons. For one, for all variants (including `base`), TiSR employs regularization by adding a squared  $\ell_1$ -norm of the parameter vector, which makes it more robust against increasing noise levels and overfitting.

Furthermore, the data is synthetically generated using ground truth expressions with normally distributed noise and no outliers. We conjecture that for problems with systematic deviations or outliers in the data, minimizing shape constraint violations during parameter identification might exhibit more significant benefits.

Finally, in situations where data is limited to a relatively small region but additional domain knowledge is available concerning some global properties of the unknown model, shape constraints are expected to be beneficial to achieve the proper extrapolation behavior. This situation, however, is not reflected in our current choice of example problems.

## 6. CONCLUSION

In this work, we propose a new way of incorporating shape constraints into SR. Our approach uniquely accounts for constraint violations during the parameter optimization phase and leverages second-order optimization along with algorithmic differentiation to enhance performance. For this purpose, we evaluate the constraint violations in a number of sample points and accumulate them into a scalar value. This value is used both as a penalty during parameter optimization as well as a separate objective during the selection process. To manage the computational expense, we propose to include the penalty term in to the parameter optimization step only for model that demonstrate good fit quality already in the absence of

constraints. This preferred variant of our algorithm is referred to as `minim_obj` throughout the paper. In our experiments, this approach is statistically significantly better in a few of our test cases compared to two baseline variants, while it is never significantly worse.

Potential future work may study the benefits of this approach for empirical data in the absence of a ground truth model.

#### REFERENCES

1. Bezanson, J.; Edelman, A.; Karpinski, S.; Shah, V. B. Julia: a fresh approach to numerical computing. *SIAM Review* **59**, 65–98. doi:[10.1137/141000671](https://doi.org/10.1137/141000671) (2017).
2. Błażdek, I.; Krawiec, K. *Solving symbolic regression problems with formal constraints Proceedings of the Genetic and Evolutionary Computation Conference* (ACM, 2019). doi:[10.1145/3321707.3321743](https://doi.org/10.1145/3321707.3321743).
3. Błażdek, I.; Krawiec, K. Counterexample-driven genetic programming for symbolic regression with formal constraints. *IEEE Transactions on Evolutionary Computation* **27**, 1327–1339. doi:[10.1109/tevc.2022.3205286](https://doi.org/10.1109/tevc.2022.3205286) (2023).
4. Damsteeg, J.-W.; Nagesh Rao, S. P.; Babuska, R. *Model-based real-time control of a magnetic manipulator system 2017 IEEE 56th Annual Conference on Decision and Control (CDC)* (IEEE, 2017). doi:[10.1109/cdc.2017.8264140](https://doi.org/10.1109/cdc.2017.8264140).
5. Deb, K.; Pratap, A.; Agarwal, S.; Meyarivan, T. A fast and elitist multi-objective genetic algorithm: NSGA-II. *IEEE Transactions on Evolutionary Computation* **6**, 182–197. doi:[10.1109/4235.996017](https://doi.org/10.1109/4235.996017) (2002).
6. Haider, C.; Kronberger, G. *Lecture Notes in Computer Science* 164–172 (Springer Nature Switzerland, 2022). doi:[10.1007/978-3-031-25312-6\\_19](https://doi.org/10.1007/978-3-031-25312-6_19).
7. Haider, C.; Olivetti de França, F.; Burlacu, B.; Kronberger, G. *Using shape constraints for improving symbolic regression models* arXiv: [2107.09458](https://arxiv.org/abs/2107.09458).
8. Haider, C.; Olivetti de França, F.; Kronberger, G.; Burlacu, B. *Comparing optimistic and pessimistic constraint evaluation in shape-constrained symbolic regression Proceedings of the Genetic and Evolutionary Computation Conference* (ACM, 2022). doi:[10.1145/3512290.3528714](https://doi.org/10.1145/3512290.3528714).
9. Kommenda, M. *Local Optimization and Complexity Control for Symbolic Regression* PhD thesis (Johannes Kepler University Linz, 2018). urn: [urn:nbn:at:at-ubl:1-21036](https://nbn-resolving.org/urn:nbn:at:at-ubl:1-21036).
10. Koza, J. R. Genetic programming as a means for programming computers by natural selection. *Statistics and Computing* **4**. doi:[10.1007/bf00175355](https://doi.org/10.1007/bf00175355) (1994).
11. Kronberger, G.; Olivetti de França, F.; Burlacu, B.; Haider, C.; Kommenda, M. Shape-constrained symbolic regression—improving extrapolation with prior knowledge. *Evolutionary Computation* **30**, 75–98. doi:[10.1162/evco\\_a.00294](https://doi.org/10.1162/evco_a.00294) (2022).
12. Kubalík, J.; Derner, E.; Babuška, R. *Symbolic regression driven by training data and prior knowledge Proceedings of the 2020 Genetic and Evolutionary Computation Conference* (ACM, 2020). doi:[10.1145/3377930.3390152](https://doi.org/10.1145/3377930.3390152).
13. La Cava, W.; Orzechowski, P.; Burlacu, B.; Olivetti de França, F.; Virgolin, M.; Jin, Y.; Kommenda, M.; Moore, J. H. *Contemporary symbolic regression methods and their relative performance* arXiv: [2107.14351](https://arxiv.org/abs/2107.14351).



14. Li, L.; Fan, M.; Singh, R.; Riley, P. *Neural-guided symbolic regression with asymptotic constraints* arXiv: [1901.07714](https://arxiv.org/abs/1901.07714).
15. Martinek, V.; Frotscher, O.; Richter, M.; Herzog, R. *Introducing thermodynamics-informed symbolic regression – a tool for thermodynamic equations of state development* arXiv: [2309.02805](https://arxiv.org/abs/2309.02805).
16. Martins, J. R. R. A.; Ning, A. *Engineering Design Optimization* doi:[10.1017/9781108980647](https://doi.org/10.1017/9781108980647) (Cambridge University Press, 2021).
17. Mogensen, P. K.; Riseth, A. N. Optim: A mathematical optimization package for Julia. *Journal of Open Source Software* **3**, 615. doi:[10.21105/joss.00615](https://doi.org/10.21105/joss.00615) (2018).
18. Piringer, D.; Wagner, S.; Haider, C.; Fohler, A.; Silber, S.; Affenzeller, M. *Lecture Notes in Computer Science* 155–163 (Springer Nature Switzerland, 2022). doi:[10.1007/978-3-031-25312-6\\_18](https://doi.org/10.1007/978-3-031-25312-6_18).
19. Reinbold, P. A. K.; Kageorge, L. M.; Schatz, M. F.; Grigoriev, R. O. Robust learning from noisy, incomplete, high-dimensional experimental data via physically constrained symbolic regression. *Nature Communications* **12**. doi:[10.1038/s41467-021-23479-0](https://doi.org/10.1038/s41467-021-23479-0) (2021).
20. Revels, J.; Lubin, M.; Papamarkou, T. *Forward-mode automatic differentiation in Julia* arXiv: [1607.07892](https://arxiv.org/abs/1607.07892).
21. Schmidt, M.; Lipson, H. *Genetic Programming Theory and Practice VIII* (eds Riolo, R.; McConaghy, T.; Vladislavleva, E.) 129–146 (Springer New York, 2010). doi:[10.1007/978-1-4419-7747-2\\_8](https://doi.org/10.1007/978-1-4419-7747-2_8).
22. Virgolin, M.; Pissis, S. P. *Symbolic regression is NP-hard* arXiv: [2207.01018](https://arxiv.org/abs/2207.01018).
23. Zille, H.; Evrard, F.; Reuter, J.; Mostaghim, S.; van Wachem, B. *Assessment of multi-objective and coevolutionary genetic programming for predicting the Stokes flow around a sphere 14th International Conference on Evolutionary and Deterministic Methods for Design, Optimization and Control* (Institute of Structural Analysis and Antiseismic Research, National Technical University of Athens, 2021). doi:[10.7712/140121.7959.18341](https://doi.org/10.7712/140121.7959.18341).

(V. Martinek) INTERDISCIPLINARY CENTER FOR SCIENTIFIC COMPUTING, HEIDELBERG UNIVERSITY, 69120 HEIDELBERG, GERMANY  
*Email address:* [viktor.martinek@iwr.uni-heidelberg.de](mailto:viktor.martinek@iwr.uni-heidelberg.de)

(J. Reuter) OTTO VON GUERICKE UNIVERSITY, FACULTY OF COMPUTER SCIENCE, CHAIR OF COMPUTATIONAL INTELLIGENCE, 39106 MAGDEBURG, GERMANY  
*Email address:* [julia.reuter@ovgu.de](mailto:julia.reuter@ovgu.de)

(O. Frotscher) FACULTY OF MECHANICAL ENGINEERING, UNIVERSITY OF TECHNOLOGY CHEMNITZ, APPLIED THERMODYNAMICS, 09107 CHEMNITZ, GERMANY  
*Email address:* [ophelia.frotscher@mb.tu-chemnitz.de](mailto:ophelia.frotscher@mb.tu-chemnitz.de)

(S. Mostaghim) OTTO VON GUERICKE UNIVERSITY, FACULTY OF COMPUTER SCIENCE, CHAIR OF COMPUTATIONAL INTELLIGENCE, 39106 MAGDEBURG, GERMANY  
*Email address:* [sanaz.mostaghim@ovgu.de](mailto:sanaz.mostaghim@ovgu.de)

(M. Richter) FACULTY OF MECHANICAL ENGINEERING, UNIVERSITY OF TECHNOLOGY CHEMNITZ, APPLIED THERMODYNAMICS, 09107 CHEMNITZ, GERMANY  
*Email address:* [m.richter@mb.tu-chemnitz.de](mailto:m.richter@mb.tu-chemnitz.de)

(R. Herzog) INTERDISCIPLINARY CENTER FOR SCIENTIFIC COMPUTING, HEIDELBERG UNIVERSITY, 69120 HEIDELBERG, GERMANY  
*Email address:* [roland.herzog@iwr.uni-heidelberg.de](mailto:roland.herzog@iwr.uni-heidelberg.de)